First-principles study of the structural, elastic, and optical properties for $Sr_{0.5}Ca_{0.5}TiO_3$*

Yang Chun-Yan(杨春燕) and Zhang Rong(张 蓉)†

Key Laboratory of Space Applied Physics and Chemistry, Ministry of Education, Northwestern Polytechnical University, Xi'an 710072, *China*

(Received 1 April 2013; revised manuscript received 20 May 2013; published online 10 December 2013)

A detailed theoretical study of the structural, elastic, and optical properties for $Sr_{0.5}Ca_{0.5}TiO_3$ is carried out by first-principles calculations. The band structure exhibits a direct bandgap of 2.08 eV at the Γ point in the Brillouin zone. The bulk modulus, shear modulus, Young's modulus, and Poisson's ratio are derived based on the calculated elastic constants. The bulk modulus $B = 153$ GPa and shear modulus $G = 81$GPa are in good agreement with available experimental data. Poisson's ratio $\nu = 0.275$ suggests that $Sr_{0.5}Ca_{0.5}TiO_3$ should be classified as being a ductile material. Using the electronic band structure and density of states, we analyze the interband contribution to the optical properties. The real and imaginary parts of the dielectric function, as well as the optical properties such as the optical absorption coefficient, refractive index, extinction coefficient, and energy-loss spectrum are calculated. The static dielectric constant $\varepsilon_1(0)$ and the refractive index $n(0)$ are also investigated.

Keywords: first-principles, electronic structure, elastic properties, optical properties

PACS: 63.20.dk, 73.22.–f, 62.20.D–, 78.20.–e **DOI:** 10.1088/1674-1056/23/2/026301

1. Introduction

The $Sr_{1-x}Ca_xTiO_3$ (SCT) solid solution has attracted considerable attention[1–7] since Bednorz and Muller[8] substituted a number of Sr^{2+} ions by Ca^{2+} in $SrTiO_3$ (ST) for $0.0018 < x < 0.016$. In the whole composition range of $0 \leq x \leq 1$, the SCT phase diagram shows a cubic Pm-$3m$ phase, a tetragonal $I4/mcm$ phase and at least four different types of orthorhombic phases.[9,10] The structural phase transitions that mainly arise from rotations of TiO_6 octahedra are usually described by Glazer formalism.[11,12] At room temperature, the structure of SCT is cubic in a range of $0 \leq x < 0.06$,[9,13] while most of the researchers proposed a space group $I4/mcm$ when $0.06 \leq x \leq 0.35$.[14–17] Yamanaka *et al.*[16] proposed the orthorhombic $Pbnm$ space group for $x \geq 0.45$. Granicher and Jakits[18] reported on the $Bmmb$ space group corresponding to the 'nearly cubic' phase for the composition range $0.35 \leq x \leq 0.60$.

Recently, there has been an increasing growth of first-principles calculations in the field of electronic materials, which has the advantage of no a priori assumption on the mechanism of interactions.[19–22] The structure of $Sr_{0.5}Ca_{0.5}TiO_3$ is identical to that of $CaTiO_3$ with $Pbnm$ space group. However, it is difficult to determine the relationship between structure and property. The previous studies aimed at identifying the crystal structure and lattice properties of unstrained $Sr_{0.5}Ca_{0.5}TiO_3$.[23–25] Ashman[26] reported on the ferroelectricity in strained $Sr_{0.5}Ca_{0.5}TiO_3$ from first principles and found that $Sr_{0.5}Ca_{0.5}TiO_3$ exhibits polarizations ranging from 0.08 C/m^2 in the lowest energy configuration to about 0.26 C/m^2 in the higher energy configurations. However, less systematic theoretical studies have been performed on the electronic structure, elastic, and optical properties from first principles.

In the present study, the electronic structure, elastic, and optical properties for $Sr_{0.5}Ca_{0.5}TiO_3$ are studied by first-principles calculations in the framework of density functional theory (DFT) using the virtual-crystal approximation (VCA). The crystal structure of $Sr_{0.5}Ca_{0.5}TiO_3$ is optimized and the electronic structures are discussed. The values of elastic constants c_{ij} are then calculated. The bulk modulus B, shear modulus G, Young's modulus Y, and Poisson's ratio ν are derived based on the values of c_{ij}. The brittleness and plasticity are also discussed. Then, the optical transition and optical properties, including dielectric function ε, optical absorption coefficient I, refractive index n, extinction coefficient k, and energy-loss spectrum L, are analyzed.

2. Details of first-principles calculations

The calculations in this work are performed using CASTEP code,[27,28] which is based on density functional theory. The generalized gradient approximation (GGA)[29] in the scheme of Perdew–Burke–Ernzerhof (PBE)[30] is used to describe the exchange–correlation functional. The interactions between electrons and core ions are treated with ultrasoft pseudopotentials.[31,32] Pseudo-atomic calculations are performed for Ca $3s^23p^64s^2$, Sr $4s^24p^65s^2$, Ti $3s^23p^63d^24s^2$, and O $2s^22p^4$ electronic configurations. A planewave cutoff energy of 340 eV is employed in the calculations. This value

*Project supported by the National Natural Science Foundation of China (Grant No. 51074129).

†Corresponding author. E-mail: xbwl01@nwpu.edu.cn

assures a high-level convergence for all parameters: the total-energy difference is convergent within 1.0×10^{-5} eV/atom, the maximum Hellmann–Feynman force within 0.03 eV/Å, the maximum stress within 0.05 GPa, and the maximum atom displacement within 1.0×10^{-3} Å. The Brillouin zone sampling is carried out using $5\times5\times2$ Monkhorst–Pack k-mesh.[33]

3. Results and discussion

3.1. Crystal structure and electronic properties

The initial unit cell of orthorhombic $Sr_{0.5}Ca_{0.5}TiO_3$ is built according to the experimental data[16] as shown in Fig. 1. For the treatment of the disordered $Sr_{0.5}Ca_{0.5}TiO_3$ compound, we use the virtual-crystal approximation (VCA). The equilibrium lattice parameters are optimized by minimizing the crystal total energy.

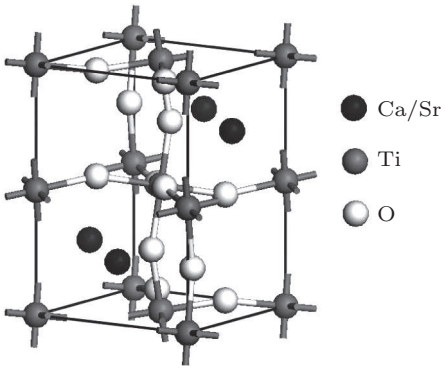

Fig. 1. Crystal structure of $Sr_{0.5}Ca_{0.5}TiO_3$.

Electronic band structure and density of states (DOS) often provide sufficient information about the electronic properties of a material. The band structure of $Sr_{0.5}Ca_{0.5}TiO_3$ is calculated along the highly symmetric directions in the first Brillouin zone based on the equilibrium structure and the result is given in Fig. 2. The Fermi energy level E_f is chosen to be located at the position of 0 eV. The valence bands appear from -4.30 eV to 0 eV, while the conduction bands appear from 2.08 eV onwards. Near the Fermi energy level, the maximum energy occurs at the Γ point and gives rise to a direct bandgap of 2.08 eV.

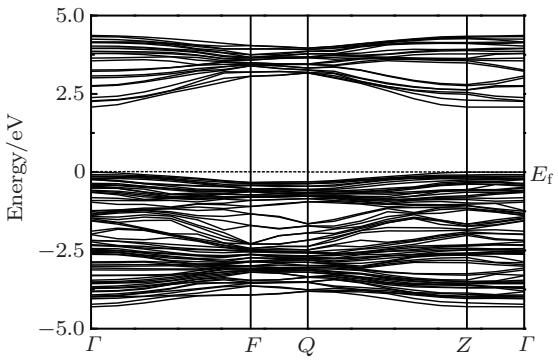

Fig. 2. Electronic band structure of $Sr_{0.5}Ca_{0.5}TiO_3$.

The total and partial electronic density of states for $Sr_{0.5}Ca_{0.5}TiO_3$ are shown in Fig. 3 which can be mainly divided into four parts. The lowest-lying states (from -20.31 eV to -18.28 eV) stem from the Ca p states. The states in a higher energy range from -17.77 eV to -13.00 eV are essentially contributed by the Sr p and O s states. It is noted that there is an obvious hybridization between Sr p and O s orbitals. States in a range from -4.82 eV to 0 eV mainly come from the O p and Ti d states, with slight contributions from Ti p states and the top of the valence band is dominated by O p states. The forth part extending from 1.55 eV to 5.03 eV is mainly composed of Ti d and O p states, which contribute to the bottom of the conduction band.

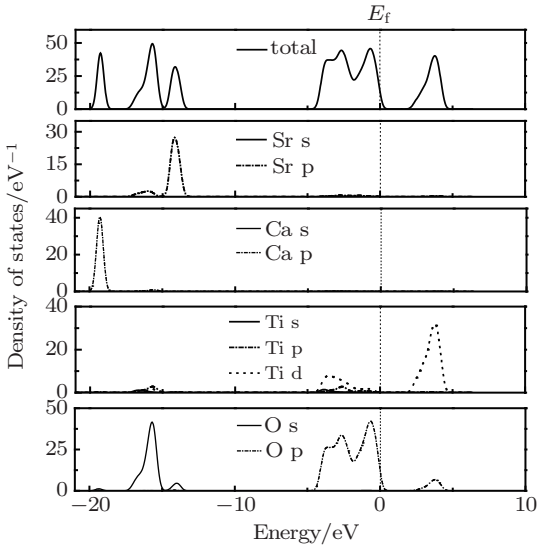

Fig. 3. Total and partial electronic density of states of $Sr_{0.5}Ca_{0.5}TiO_3$.

3.2. Elastic properties

The elastic constants are important parameters that describe the reliability of both physical models and engineering application at the atomic level.[34,35] We use the standard stress–strain method to derive all of the elastic constants. This method is based on constructing a set of linear equations for several deformations of the unit cell. The elastic constants c_{ij}'s are directly calculated by CASTEP code, in which the stress with respect to the finite strain is defined as

$$\sigma_i = \sum_{j=1}^{6} c_{ij}\varepsilon_j, \tag{1}$$

where σ_i ($i = 1$–6) are the stress components and ε_j ($j = 1$–6) are the applied small strains, and c_{ij}'s are the elastic constants of the crystal.

Once the elastic constants are obtained, the polycrystalline elastic moduli can be calculated by Reuss–Voigt–Hill approach.[36,37] The bulk modulus B represents the resistance to fracture, while the shear modulus G represents the resis-

tance to plastic deformation. They can be written as

$$B = (B_{\rm R} + B_{\rm V})/2, \tag{2}$$

$$G = (G_{\rm R} + G_{\rm V})/2, \tag{3}$$

where R and V represent Reuss and Voigt boundary, respectively. $Sr_{0.5}Ca_{0.5}TiO_3$ has an orthorhombic structure, and correspondingly has nine independent elastic tensor elements. For an orthorhombic system[38]

$$9B_{\rm V} = (c_{11}+c_{22}+c_{33})+2(c_{12}+c_{13}+c_{23}), \tag{4}$$

$$15G_{\rm V} = (c_{11}+c_{22}+c_{33})+3(c_{44}+c_{55}+c_{66}) - (c_{12}+c_{13}+c_{23}), \tag{5}$$

$$1/B_{\rm R} = (s_{11}+s_{22}+s_{33})+2(s_{12}+s_{13}+s_{23}), \tag{6}$$

$$15/G_{\rm R} = 4(s_{11}+s_{22}+s_{33})-4(s_{12}+s_{13}+s_{23}) +3(s_{44}+s_{55}+s_{66}), \tag{7}$$

where s_{ij} is the element of elastic compliance tensor.

The Young's modulus Y and Poisson's ratio ν are often used for characterizing the hardness values of polycrystalline materials. The larger the Young's modulus, the better the ductility is. Poisson's ratio v provides more information about the bonding forces than any other elastic properties. The lower and upper limits for a central force solid are 0.25 and 0.5, respectively. These quantities can be calculated in terms of B and G using the following relations:[38]

$$Y = 9BG/(G+3B), \tag{8}$$

$$\nu = (3B-2G)/[2(3B+G)]. \tag{9}$$

The calculated elastic constants of $Sr_{0.5}Ca_{0.5}TiO_3$ are presented in Table 1. The calculated c_{11}, c_{22}, and c_{33} are large among the results, which indicates that this crystal is incompressible under uniaxial stress along x, y or z axis. In addition, it is found that the elastic constants satisfy the following generalized elastic stability criteria for orthorhombic crystals:[39]

$$\begin{aligned} &c_{ii} > 0, \quad (i = 1,2,3,4,5,6)\\ &[c_{11}+c_{22}+c_{33}+2(c_{12}+c_{13}+c_{23})] > 0,\\ &(c_{11}+c_{22}-2c_{12}) > 0,\\ &(c_{11}+c_{33}-2c_{13}) > 0,\\ &(c_{22}+c_{33}-2c_{23}) > 0. \end{aligned} \tag{10}$$

Table 1. Elastic constants (in GPa) of $Sr_{0.5}Ca_{0.5}TiO_3$ from first-principles calculations.

c_{11}	c_{22}	c_{33}	c_{44}	c_{55}	c_{66}	c_{12}	c_{13}	c_{23}
286	256	279	114	97	41	76	124	82

The calculated polycrystalline moduli are presented in Table 2. The bulk modulus $B = 153$ GPa and shear modulus $G = 81$ GPa are in good agreement with the available experimental data.[40] The ratio of bulk modulus to shear modulus of polycrystalline phases, B/G, can be taken as prediction of the ductile or brittle behavior. A high B/G ratio is associated with ductility, whereas a low value corresponds to the brittle nature. The critical value that separates brittleness from ductility is about 1.75. The values of B/G, Young's modulus Y, and Poisson's ratio ν for $Sr_{0.5}Ca_{0.5}TiO_3$ are 1.889, 282 GPa, and 0.275, respectively. It is suggested that $Sr_{0.5}Ca_{0.5}TiO_3$ should be classified as a ductile material.

Table 2. Calculated values of bulk modulus B (in GPa), shear modulus G (in GPa), B/G, Young's modulus Y (in GPa), and Poisson's ratio ν for $Sr_{0.5}Ca_{0.5}TiO_3$.

	B	G	B/G	Y	ν
Calc.	153	81	1.889	282	0.275
Expt.[40]	152	88			
	148	88			

3.3. Optical properties

The optical properties of matter can be described by the transverse dielectric function $\varepsilon(q,\omega)$, where q is the momentum transfer in the photon–electron interaction and ω is the energy transfer. In the present study, electric-dipole approximation is adopted, according to which the momentum transfer from the initial state to the final state is neglected. The real and imaginary parts of $\varepsilon(\omega)$ are often referred to as $\varepsilon_1(\omega)$ and $\varepsilon_2(\omega)$, respectively, which gives $\varepsilon(\omega) = \varepsilon_1(\omega) + {\rm i}\varepsilon_2(\omega)$. In general, there are two contributions to $\varepsilon(\omega)$, namely intraband and interband transitions. The contribution from intraband transitions is important only for metals, while the interband transitions can be split into direct and indirect transitions. The imaginary part $\varepsilon_2(\omega)$ is calculated from the electronic structure and the momentum matrix elements, and is given by

$$\varepsilon_2(\omega) = \frac{Ve^2}{2\pi\hbar m^2\omega^2}\int {\rm d}^3\kappa |\langle\psi_{\rm C}|p|\psi_{\rm V}\rangle|^2 \cdot\delta(E_{\rm C}-E_{\rm V}-\hbar\omega), \tag{11}$$

where $\psi_{\rm C}$ and $\psi_{\rm V}$ are the wave functions in the conduction and valence band respectively, p is the momentum operator, ω is the photon frequency, and $\hbar$ is reduced Planck's constant.

The real part of the frequency-dependent response functions $\varepsilon_1(\omega)$ can be obtained from the imaginary part $\varepsilon_2(\omega)$ by using the Kramers–Kronig[41] transformation

$$\varepsilon_1(\omega) = 1+\frac{2}{\pi}P\int_0^\infty \frac{\varepsilon_2(\omega'){\rm d}\omega'}{(\omega')^2-(\omega)^2}, \tag{12}$$

where P is the principle value of the integral.

The real and imaginary parts of the dielectric function are shown in Fig. 4. It can be seen that the behaviors of $\varepsilon_1(\omega)$ and $\varepsilon_2(\omega)$ are rather similar. For the real part $\varepsilon_1(\omega)$, there are mainly three peaks located at 2.86 eV, 18.58 eV, and 35.03 eV, respectively. The most important quantity obtained from the real dielectric function is the zero frequency limit $\varepsilon_1(0)$ and the calculated value is 3.79. Additionally, $\varepsilon_1(\omega)$ is negative in an

energy range from 4.39 eV to 8.28 eV because the electromagnetic wave is damped, and $\varepsilon_1(\omega) = 0$ because longitudinally polarized waves are possible. In the spectrum of $\varepsilon_2(\omega)$, there are three peaks located at 4.11 eV, 19.37 eV, and 36.09 eV. The peak at 4.11 eV should mainly be caused by electronic transitions between O 2p states in the highest valence band and Ti 3d states in the lowest conduction band. The lowest peak at 19.37 eV can be due to the electronic transition between the Sr 4p and Ti 3d states, and the highest peak at 36.09 eV mainly derives from the electronic transition between Ti 3p and Ti 3d states.

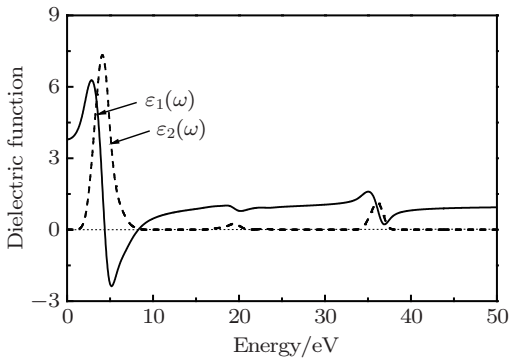

Fig. 4. Real and imaginary dielectric functions of $Sr_{0.5}Ca_{0.5}TiO_3$.

Figure 5 shows the calculated energy dependences of absorption coefficient $I(\omega)$, refractive index $n(\omega)$, extinction coefficient $k(\omega)$, and energy-loss spectrum $L(\omega)$ respectively. The corresponding absorption coefficient is calculated by[42]

$$I(\omega) = \sqrt{2}(\omega)(\sqrt{\varepsilon_1(\omega)^2 + \varepsilon_2(\omega)^2} - \varepsilon_1(\omega))^{1/2}. \quad (13)$$

The results are illustrated in Fig. 5(a). It can be seen that the absorption spectrum starts from about 0.45 eV and there are three peaks in the whole energy range, in which the maximum value of absorption appears at an energy of 36.40 eV. Although our results cannot be compared with experimental ones due to the lack of experimental data concerning absorption spectrum in the energy range investigated in this work, they can be expected to be verified by future experimental investigations.

The refractive index $n(\omega)$ and extinction coefficient $k(\omega)$ are shown in Figs. 5(b) and 5(c) respectively. It is found that the maximum of $n(\omega)$ is about 2.59 at 3.14 eV and the minimum of $n(\omega)$ is about 0.09 at 8.09 eV. The static refractive index $n(0)$ is 1.94. At higher energy, the refractive index is about 1.00. The extinction coefficient $k(\omega)$ directly describes the attenuation of the electromagnetic waves within the medium. For $Sr_{0.5}Ca_{0.5}TiO_3$, this coefficient has large value in an energy range of 0.70 eV to 9.56 eV.

The peaks in $L(\omega)$ spectrum represent the characteristics associated with plasma resonance and the corresponding frequency is the so-called plasma frequency, above and below which the material exhibits dielectric and metallic properties, respectively. The sharp peak is associated with the plasma oscillation and indicates the point of transition from metallic to dielectric property. From Fig. 5(d), it can be seen that the plasma frequency for $Sr_{0.5}Ca_{0.5}TiO_3$ appears at the position of 8.31 eV.

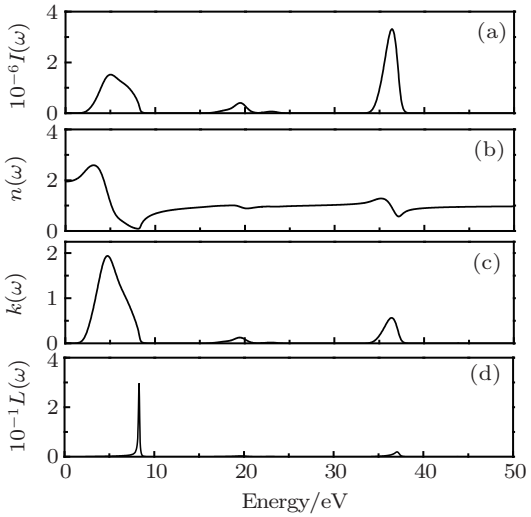

Fig. 5. Calculated optical properties of $Sr_{0.5}Ca_{0.5}TiO_3$. (a) Absorption coefficient I, (b) refractive index n, (c) extinction coefficient k, and (d) energy-loss spectrum L.

4. Conclusions

The electronic structure, elastic, and optical properties of $Sr_{0.5}Ca_{0.5}TiO_3$ are presented using the first-principles method based on density functional theory. The results are obtained as follows.

(i) The band structure shows that $Sr_{0.5}Ca_{0.5}TiO_3$ has a direct bandgap of 2.08 eV at the Γ point in the Brillouin zone. The calculations of band structure and density of states (DOS) reveal the acceptable characteristics.

(ii) The nine independent elastic constants are determined. The values in three major axes are $c_{11} = 286$ GPa, $c_{22} = 256$ GPa, and $c_{33} = 279$ GPa which indicate that this crystal is incompressible under uniaxial stress along x, y or z axis. The Bulk modulus $B = 153$ GPa and shear modulus $G = 81$ GPa accord well with available experimental data. The ratio of $B/G = 1.889$, Young's modulus $Y = 282$ GPa, and Poisson ratio $\nu = 0.275$ show that $Sr_{0.5}Ca_{0.5}TiO_3$ behaves as a ductile material.

(iii) The dielectric function, absorption coefficient, refractive index, extinction coefficient, and energy-loss spectrum are also calculated. The static dielectric constant and static refractive index are 3.79 and 1.94, respectively. The plasma frequency is estimated to appear at the position of 8.31 eV.

Acknowledgment

The authors thank the Northwestern Polytechnical University High Performance Computing Center for the allocation of computing time and resources. One of the authors (Yang) is very grateful to Mr. Li Liu-Hui for his helpful discussion.

References

[1] Mishra S K, Ranjan R, Pandey D, Ouillon R, Pinan-Lucarre J P, Ranson P and Pruzan Ph 2005 *J. Solid State Chem.* **178** 2846
[2] Mishra S K, Ranjan R, Pandey D and Kennedy B J 2002 *J. Appl. Phys.* **91** 4447
[3] Ranjan R and Pandey D 2001 *J. Phys.: Condens. Matter* **13** 4251
[4] Ouillon R, Pinan-Lucarre J P, Ranson P, Pruzan Ph, Mishra S K, Ranjan R and Pandey D 2002 *J. Phys.: Condens. Matter* **14** 2079
[5] Becerro A I, Redfern S A T, Carpenter M A, Knight K S and Seifert F 2002 *J. Solid State Chem.* **167** 459
[6] Ranjan R, Pandey D and Lalla N P 2000 *Phys. Rev. Lett.* **84** 3726
[7] Howard C J, Withers R L and Kennedy B J 2001 *J. Solid State Chem.* **160** 8
[8] Bednorz J G and Muller K A 1984 *Phys. Rev. Lett.* **52** 2289
[9] Ranjan R, Pandey D, Schuddinck W, Richard O, De Meulenaere P, Van Landuyt J and Van Tendeloo G 2001 *J. Solid State Chem.* **162** 20
[10] Ranjan R, Pandey D, Siruguri V, Krishna P S R and Paranjpe S K 1999 *J. Phys.: Condens. Matter* **11** 2233
[11] Glazer A M 1972 *Acta Cryst. B* **28** 3384
[12] Glazer A M 1975 *Acta Cryst. A* **31** 756
[13] Ranjan R and Pandey D 2001 *J. Phys.: Condens. Matter* **13** 4239
[14] Ball C J, Begg B D, Cookson D J, Thorogood G J and Vance E R 1998 *J. Solid State Chem.* **139** 238
[15] Qin S, Becerro A I, Seifert F, Gottsmann J and Jiang J 2000 *J. Mater. Chem.* **10** 1609
[16] Yamanaka T, Hirai N and Komatsu Y 2002 *Am. Mineral.* **87** 1183
[17] Qin S, Wu X, Seifert F and Becerro A I 2002 *J. Chem. Soc., Dalton Trans.* **19** 3751
[18] Granicher H and Jakits O 1954 *Nuovo Cimento Suppl.* **11** 480
[19] Yang Z J, Guo Y D, Linghu R F and Yang X D 2012 *Chin. Phys. B* **21** 036301
[20] Zhu F, Dong S and Cheng G 2011 *Chin. Phys. B* **20** 077103
[21] Liu L Y, Wang R Z, Zhu M K and Hou Y D 2013 *Chin. Phys. B* **22** 036401
[22] Zhang S, Pang H, Fang Y and Li F S 2010 *Chin. Phys. B* **19** 127102
[23] Carpenter M A, Howard C J, Knight K S and Zhang Z 2006 *J. Phys.: Condens. Matter* **18** 10725
[24] Woodward D I, Wise P L, Lee W E and Reaney I M 2006 *J. Phys.: Condens. Matter* **18** 2401
[25] Hui Q, Dove M T, Tucker M G, Redfern S A T and Keen D A 2007 *J. Phys.: Condens. Matter* **19** 335214
[26] Ashman C R 2010 *Phys. Rev. B* **82** 024112
[27] Clark S J, Segall M D, Pickard C J, Hasnip P J, Probert M I J, Refson K and Payne M C 2005 *Z. Kristallogr.* **220** 567
[28] Segall M D, Lindan P J D, Probert M J, Pickard C J, Hasnip P J, Clark S J and Payne M C 2002 *J. Phys.: Condens. Matter* **14** 2717
[29] Pack J D and Monkhors H J 1977 *Phys. Rev. B* **16** 1748
[30] Perdew J P, Burke K and Ernzerhof M 1996 *Phys. Rev. Lett.* **77** 3865
[31] Vanderbilt D 1990 *Phys. Rev. B* **41** 7892
[32] Perdew J P, Chevary J A, Vosko S H, Jaskson K A, Pederson M P, Singh D J and Fiolhais C 1992 *Phys. Rev. B* **46** 6671
[33] Monkhorst H J and Pack J D 1976 *Phys. Rev. B* **13** 5188
[34] Panda K B and Ravi Chandran K S 2006 *Acta Mater.* **54** 1641
[35] Wu Q and Li S S 2012 *Comput. Mater. Sci.* **53** 436
[36] Chung D H and Buessem W R 1967 *J. Appl. Phys.* **38** 2010
[37] Chung D H and Buessem W R 1967 *J. Appl. Phys.* **38** 2535
[38] Hill R 1952 *Proc. Phys. Soc. A* **65** 349
[39] Wu Z, Zhao E, Xiang H, Hao X, Liu X and Meng J 2007 *Phys. Rev. B* **76** 054115
[40] Walsh J N, Taylor P A, Buckley A, Darling T W, Schreuer J and Carpenter M A 2008 *Phys. Earth Planet. Inter.* **167** 110
[41] Kohn W and Sham L J 1965 *Phys. Rev.* **140** A1133
[42] Cao X R, Li Y S, Cheng X and Zhang Y 2012 *Comput. Mater. Sci.* **54** 84